



An improved subgrid channel model with upwind-form artificial diffusion for river hydrodynamics and floodplain inundation simulation

Youtong Rong, Paul Bates, and Jeffrey Neal

School of Geographical Sciences, University of Bristol, Bristol, BS8 1QU, UK

Correspondence: Youtong Rong (youtong.rong@bristol.ac.uk)

Received: 23 September 2022 – Discussion started: 10 October 2022

Revised: 3 May 2023 – Accepted: 8 May 2023 – Published: 13 June 2023

Abstract. An accurate estimation of river channel conveyance capacity and the water exchange at the river–floodplain interfaces is pivotal for flood modelling. However, in large-scale models limited grid resolution often means that small-scale river channel features cannot be well-represented in traditional 1D and 2D schemes. As a result instability over river and floodplain boundaries can occur, and flow connectivity, which has a strong control on the floodplain hydraulics, is not well-approximated. A subgrid channel (SGC) model based on the local inertial form of the shallow water equations, which allows utilization of approximated subgrid-scale bathymetric information while performing very efficient computations, has been proposed as a solution, and it has been widely applied to calculate the wetting and drying dynamics in river–floodplain systems at regional scales. Unfortunately, SGC approaches to date have not included the latest developments in numerical solutions of the local inertial equations, and the original solution scheme was reported to suffer from numerical instability in low-friction regions such as urban areas. In this paper, for the first time, we implement a newly developed diffusion and explicit adaptive weighting factor in the SGC model. Adaptive artificial diffusion is explicitly included in the form of an upwind solution scheme based on the local flow status to improve the numerical flux estimation. A structured sequence of numerical experiments is performed, and the results confirm that the new SGC model improved the model performance in terms of water level and inundation extent, especially in urban areas where the Manning parameter is less than $0.03 \text{ m}^{-1/3} \text{ s}$. By not compromising computational efficiency, this improved SGC model is a compelling alternative for river–floodplain modelling, particularly in large-scale applications.

1 Introduction

Recent flood events and climate change concerns have boosted the requirements for hydraulic models with fast and accurate calculation of both spatial and temporal flow dynamics in river–floodplain systems (Jongman et al., 2012; Edmonds et al., 2020; McMichael et al., 2020). Flood risk assessment based on the output of hydrodynamic simulation models has been proven effective to prepare for disasters and can facilitate good decision-making at local, regional, and national levels of government, reducing the risk posed by flood hazards (Al Baky et al., 2020). There is thus an increasing demand for flood modelling studies that can accurately represent the dominant hydrodynamic process during flood events and provide recommendations for mitigating measures to alleviate the impact of potential flooding (Paiva et al., 2011; Yamazaki et al., 2014).

Though the large magnitude associated with most floods might appear to overshadow the impact of river channel bathymetry incorporation, the channel in fact still conveys a significant proportion of the flow during a flood event because of the much higher channel velocity compared to the floodplain (Grimaldi et al., 2018; Neal et al., 2015). As a result, accurate estimates of river conveyance capacity and cross-section depth values deserve more attention than accurate predictions of far-field flood elevations, and physics-based hydrodynamic model performance can be improved in terms of wave propagation speed and inundation extent through good representation of the river channel (Fewtrell et al., 2011). For example, the average predicted inundation extent decreased by more than 30 % and average water surface elevation dropped by 0.5 m after incorporating bathymetric

data in a hydrodynamic model of Strouds Creek in North Carolina (Cook and Merwade, 2009). Changes in inundation extent due to proper accounting of river channel conveyance are much greater for areas with a flat topography. Crucial physical aspects of river hydraulics, like backwater effects and looped stage–discharge relations, are omitted without the inclusion of the river bathymetry or even with simplified river-routing models (e.g. Muskingum–Cunge method, kinematic hydraulic model). Such a simplified hydrodynamic model therefore cannot resolve inundation patterns necessary to understand associated risks locally (Schumann et al., 2013). Furthermore, floodplain water levels cannot be assumed to be the same as channel water levels because of water storage on floodplains, and complex and nonlinear interactions between the channel and floodplain are to be expected (Alsdorf et al., 2007; Trigg et al., 2009, 2012). Efficient incorporation of river channel bathymetry in flood inundation models is therefore fundamental for modelling the mass and momentum exchange at the river–floodplain interface, dynamic wetting and drying process on the floodplain, and the wave propagation characteristics.

Given that river channel flows are an essential component in flood modelling, several approaches have been implemented to integrate river hydraulics into hydrodynamic models:

1. a 1D river hydraulic model without a floodplain or with extended cross-sections to approximate floodplain storage and river channel conveyance in 1D;
2. a 2D floodplain inundation model representing the channel and floodplain in a single discretization;
3. 1D and 2D representation with main channels and a floodplain; and
4. 1D and 2D representation with subgrid-scale simplified channels.

By omitting the floodplain inundation process, 1D river hydraulic models are a lightweight alternative to a 2D hydrodynamic model framework. Together with a volume storage grid or an extended cross-section to approximate the floodplain storage and conveyance, the 1D model has been successfully implemented to assess flood risk in major rivers globally (Yamazaki et al., 2011; Rudari et al., 2015). However, 1D models are incapable of accommodating the real physical and hydrodynamic conditions required to represent a number of river processes (Merwade et al., 2008). Realistic flow inundation process and channel–floodplain momentum exchange cannot be obtained without the floodplain component. With the emphasis on the floodplain inundation process, 2D models provide a solution which can either ignore the river conveyance capacity or represent the channel with a fine grid resolution at the cost of substantially increasing computational time, even with an unstructured discretization of space. This costly and unnecessary grid refinement

in the channel region has hampered the further application of full 2D models, especially for resource-intensive large-scale flood inundation simulation.

The combination of a 1D model in the channel and a 2D model for the floodplain offers the benefits of capturing 2D processing on the floodplain whilst minimizing the computational costs and below water line data requirements in the river channel. However, the troublesome interactions at the river–floodplain interface demand extra attention due to their effect on the mass and momentum balance there; otherwise, a divergent outcome can easily be acquired. Furthermore, 1D and 2D models can have limited capacity to properly represent minor river channels that can have a strong control on the floodplain hydraulics, and this restricts the further improvement of 1D and 2D model efficiency. Since models missing either the channel network or floodplain component have reduced predictive skill at large scales (Neal et al., 2012), research has sought to identify an efficient alternative for river–floodplain modelling.

To enable a physically consistent representation of the river–floodplain system and reduce the computational burden of floodplain inundation modelling, the subgrid channel (SGC) model solving the local inertial form of the shallow water equations has been proposed, allowing the utilization of available subscale bathymetric information while performing computations on relatively coarse grids (Neal et al., 2012). Flow connectivity provided by the fine-resolution river channel network and its strong control on the floodplain hydraulics is incorporated into the model. Precise mass balance in regions where wetting and drying occurs is achieved within a well-structured, mildly nonlinear system for the discrete water surface elevation. The adoption of the subgrid method improves computing performance by roughly a factor of 20 compared with the classical 2D model based on unstructured grids (Sehili et al., 2014).

Unfortunately, SGC approaches to date have not included the latest developments in numerical solutions of the local inertial equations. Despite its high performance, the original SGC solution scheme was reported to suffer from numerical instability in low-friction regions such as urban areas (Bates et al., 2010). The problem has been tackled by introducing limited artificial diffusion in the form of weighting factors for the neighbouring flux (de Almeida et al., 2012). An explicit expression of the adaptive weighting factor depending on local velocity, flow depth, grid resolution, and time step size has also recently been developed to recognize the different diffusion needed at each iteration (Sridharan et al., 2020). This adaptive weighting factor has been shown to improve simulation of flood propagation over the floodplain, but its application to the channel hydrodynamics calculation is still lacking, as is its ability to assess the water exchange between river and floodplain. Implementation of the schemes above has also not yet been evaluated at channel confluences. This paper therefore adds this new explicitly calculated diffusion to an SGC model for the first time and also adds a further

constraint on the available range of the weighting factor to balance the contribution of the flux from the local and upwind surfaces. This enables an improved and computationally efficient solution for river–floodplain flow inundation simulation with multi-core CPUs.

The paper is structured as follows: the development of the improved SGC model is outlined in Sect. 2, with the emphasis on how to adopt the new upwind solution scheme in the discretization procedure of the governing equations. A wide range of tests are set up in Sect. 3, from steady and unsteady problems with an analytical solution to practical applications with detailed ground survey data, to evaluate the model performance quantitatively. Volume error, root mean square error (RMSE), and inundation extent are used to quantify the model accuracy compared with three other solvers which are also implemented in the LISFLOOD-FP hydrodynamic model. Conclusions are drawn in Sect. 4.

2 Methodology

The following section outlines the steps associated with including the latest development in numerical solutions of the local inertial equations in the SGC model. Procedures adopted to improve the original SGC solution schemes in the calculation of floodplain flow propagation, river hydrodynamics, and water exchange over the river–floodplain boundaries are described. These approaches have been confirmed to improve the accuracy and robustness of the solution scheme and are therefore here implemented to enhance the performance of the SGC model.

2.1 Governing equations

The subgrid channel model employs the efficient local inertial formulation of the shallow water equations to calculate the surface flux between adjacent floodplain cells and update the water depth in every structured digital elevation model (DEM) cell, as shown in Eqs. (1)–(3). The simplified governing equations are achieved by neglecting the advection term in the momentum equation from the quasi-linearized 1D Saint-Venant equations (Bates et al., 2010). For gradually varied flows wherein such approximations are not contradicted (de Almeida and Bates, 2013), these equations can efficiently yield results with accuracy comparable to the full-dynamic system (Neal et al., 2012; Rajib et al., 2020). The equations with formulae decoupled in the x and y directions can be employed directly for the calculation of flood propagation over the floodplain. A 1D interpretation of these governing equations is required for the river flow calculation, and the flow area is explicitly included in the solution scheme during the discretization process to account for precise channel conveyance capacity:

$$\frac{\partial h}{\partial t} + \frac{\partial q_x}{\partial x} + \frac{\partial q_y}{\partial y} = 0, \quad (1)$$

$$\frac{\partial q_x}{\partial t} + gh \frac{\partial(h+z)}{\partial x} + \frac{gn^2 |q_x| q_x}{h^{7/3}} = 0, \quad (2)$$

$$\frac{\partial q_y}{\partial t} + gh \frac{\partial(h+z)}{\partial y} + \frac{gn^2 |q_y| q_y}{h^{7/3}} = 0, \quad (3)$$

where h is the water depth [L], q is the discharge per unit width [$L^2 T^{-1}$], z is the bed elevation [L], g is the acceleration due to gravity [$L T^{-2}$], n is the Manning friction coefficient [$L^{-1/3} T$], x and y denote the horizontal and vertical coordinate [L], and t is the time [T].

Flood inundation models governed by local inertial equations focus on the calculation of the dominant hydrodynamics process during gradually varied and subcritical flow propagation. Accurate mass and momentum balance in shallow flows over complex geometries is ensured in the presence of wetting and drying. Compared with the full-dynamics shallow water equations (SWEs), the simplified governing equations demand fewer computational resources while still preserving the main features of the gradually varied flow field (Shaw et al., 2021). Therefore, the local inertial equations are taken as the governing equations for the calculation of flow propagation in the new SGC model. The latest developments in solution schemes for the local inertial equations are implemented to tackle the potential instability problem of the original SGC model of Bates et al. (2010).

2.2 Solution scheme for floodplain inundation calculation

The original SGC solution scheme is reported to suffer from divergence problems in urban areas with low friction, and simulation accuracy is also impacted by the original solution scheme. Improvements to the original SGC solution schemes (Eqs. 2 and 3) follow the procedure proposed by de Almeida et al. (2012), which explicitly includes artificial diffusion in the form of an upwind solution scheme. A fixed weighting factor balancing the contribution of upwind and local flow flux is necessary in this solution scheme, and repeated tests are required to determine a global optimum value for the weighting factor. Then an adaptive weighting factor depending on the local flow status is explicitly integrated to enable an automatic determination of the artificial diffusion needed to stabilize the solution scheme (Sridharan et al., 2020). By importing artificial diffusion, the explicit expression of the momentum equations in the form of the upwind scheme is acquired as shown in Eq. (4). A similar equation can be derived with the same structure to calculate the discharge in the y direction. With the upwind discharge included ($Q_{i-3/2,j}^t$ or $Q_{i+1/2,j}^t$, depending on local flow direction), the system can respond to the upwind flow flux variation with great flexibility to avoid the formulation of nonphysical water depth gradients caused by the delayed propagation of flow information in the original scheme. Imported adaptive diffusion enables oscillation-free solutions in many cases in which the original scheme has the potential to be divergent (O’Loughlin et al.,

2020; Shustikova et al., 2019; Sridharan et al., 2021).

$$Q_{i-1/2,j}^{t+\Delta t} = \begin{cases} \frac{\theta Q_{i-1/2,j}^{t+\Delta t} + (1-\theta) Q_{i-3/2,j}^{t-\Delta t} - g A_{i-1/2,j,\text{flow}}^{t-\Delta t} \Delta t S_{i-1/2,j}^{t-\Delta t}}{\left[1 + g \Delta t n_{i-1/2,j}^2 \left| \frac{Q_{i-1/2,j}^{t-\Delta t}}{A_{i-1/2,j}} \right| / \left[(h_{i-1/2,j,\text{flow}}^t)^{4/3} A_{i-1/2,j,\text{flow}}^t \right] \right]}, & \text{if } Q_{i-1/2,j}^{t-\Delta t} > 0, \\ \frac{\theta Q_{i-1/2,j}^{t+\Delta t} + (1-\theta) Q_{i+1/2,j}^{t-\Delta t} - g A_{i-1/2,j,\text{flow}}^{t-\Delta t} \Delta t S_{i-1/2,j}^{t-\Delta t}}{\left[1 + g \Delta t n_{i-1/2,j}^2 \left| \frac{Q_{i-1/2,j}^{t-\Delta t}}{A_{i-1/2,j}} \right| / \left[(h_{i-1/2,j,\text{flow}}^t)^{4/3} A_{i-1/2,j,\text{flow}}^t \right] \right]}, & \text{if } Q_{i-1/2,j}^{t-\Delta t} < 0, \\ \frac{-g A_{i-1/2,j,\text{flow}}^{t-\Delta t} \Delta t S_{i-1/2,j}^{t-\Delta t}}{\left[1 + g \Delta t n_{i-1/2,j}^2 \left| \frac{Q_{i-1/2,j}^{t-\Delta t}}{A_{i-1/2,j}} \right| / \left[(h_{i-1/2,j,\text{flow}}^t)^{4/3} A_{i-1/2,j,\text{flow}}^t \right] \right]}, & \text{if } Q_{i-1/2,j}^{t-\Delta t} = 0 \end{cases} \quad (4)$$

Here, Δx represents the horizontal dimensions of the DEM cells [L], and S is the water surface slope between two adjacent cells. A is the flow area [L²], and h is the water depth [L]. The subscript of “flow” indicates that these components vary with the flow status. Q is discharge across the cell boundaries [L³ T⁻¹]. The discharge is defined as positive if the flow direction is from west to east or from north to south, supposing that the origin of the discrete domain is located in the upper left (northwest) corner. Depending on the flow direction at the local cell interface, one of its two adjacent surfaces in the same direction is selected as the upwind flux, representing the information propagation direction of the local flow field. No artificial diffusion is included if there is no flux at the local cell interface. With the momentum equations solved based on the discharge from the last time step, local discharge representing the momentum exchange at the grid interfaces is updated, and then the cell-average water depth can be solved with Eq. (5), which is the continuity equation relating flow into a cell and its volume change.

$$h_{i,j}^{t+\Delta t} = h_{i,j}^t + \Delta t \frac{Q_{xi-1/2,j}^{t+\Delta t} - Q_{xi+1/2,j}^{t+\Delta t} + Q_{yi,j-1/2}^{t+\Delta t} - Q_{yi,j+1/2}^{t+\Delta t}}{A_{i,j}} \quad (5)$$

Following Sridharan et al. (2020), the weighting factor θ defined in Eq. (6) quantifies how much artificial diffusion is required to stabilize the solution scheme. A predefined uniform weighting factor was previously set for surface flux calculation in the original subgrid channel scheme of the LISFLOOD-FP model, and a tricky calibration was required to acquire a global optimal solution (de Almeida et al., 2012). However a global optimum solution does not guarantee the best performance of the local flow calculation, so an adaptive procedure is now implemented to determine the value of θ so that no trials and approximations are needed and the weighting factor can be updated automatically based on the local velocity, flow depth, grid resolution, and time step size (Sridharan et al., 2020), as shown in Eq. (6). An extra constraint on the feasible range of the weighting factor θ is applied in this paper to limit its minimum value to 0.7. This ensures that the local interface flux dominates the flux calculation, while artificial diffusion from upwind cannot be overused. Potential instability problems can be induced on the condition that the local flux estimation mainly depends on the upwind flow

information while ignoring the local flow status. These adaptive measures pay close attention to the change of the flow field to identify the dominant factor for updating the surface flux, thus increasing the robustness of the system. Compared with the fixed weighting factor strategy, great flexibility is incorporated without compromising the computational efficiency.

$$\theta_{i-1/2,j} = 1 - \frac{\Delta t}{\Delta x} \min \left(\frac{|q_{i-1/2,j}|}{h_{\text{flow}}}, \sqrt{g h_{\text{flow}}} \right) \quad (6)$$

2.3 Solution scheme for river hydraulics calculation

Similar procedures implemented to improve floodplain inundation calculation are applied to discretize the 1D interpolation of the local inertial equations for river hydraulics calculation. Subscale channel parameters that represent the rectangular channel flow area (A) are integrated during the discretization process, accounting for the flow conveyance capacity with subscale river width (w) and flow depth (d). The subscale representation of the channel features enables a numerically consistent representation of flow dynamics even in large-scale river–floodplain modelling. With subgrid sampling, the underlying topography dominating the river flow transport, in the form of the approximated rectangular river channel, is still utilized despite a coarser grid resolution being applied for the floodplain. This allows the user to focus details where required for inundation extent prediction without compromising computational efficiency in locations of little topographic variability. A more stable and efficient solution scheme is acquired by this means for the river hydraulics calculation (Eq. 7).

$$Q_{ci,j-1/2}^{t+\Delta t} = \begin{cases} \frac{\theta Q_{ci,j-1/2}^{t+\Delta t} + (1-\theta) Q_{c,\text{up}}^{t-\Delta t} - g A_{ci,j-1/2,\text{flow}}^{t-\Delta t} \Delta t S_{ci,j-1/2}^{t-\Delta t}}{\left[1 + g \Delta t n_{ci,j-1/2}^2 \left| \frac{Q_{ci,j-1/2}^{t-\Delta t}}{A_{ci,j-1/2}} \right| / \left[(R_{ci,j-1/2,\text{flow}}^t)^{4/3} A_{ci,j-1/2,\text{flow}}^t \right] \right]}, & \text{if } |Q_{ci,j-1/2}^{t-\Delta t}| > 0 \\ \frac{-g A_{ci,j-1/2,\text{flow}}^{t-\Delta t} \Delta t S_{ci,j-1/2}^{t-\Delta t}}{\left[1 + g \Delta t n_{ci,j-1/2}^2 \left| \frac{Q_{ci,j-1/2}^{t-\Delta t}}{A_{ci,j-1/2}} \right| / \left[(R_{ci,j-1/2,\text{flow}}^t)^{4/3} A_{ci,j-1/2,\text{flow}}^t \right] \right]}, & \text{if } Q_{ci,j-1/2}^{t-\Delta t} = 0 \end{cases} \quad (7)$$

Here, i and j denote the column and row index of the grid, respectively, which is the same as the 2D base model. The subscript c denotes the channel flow discharge to distinguish it from the floodplain surface flux. Only if two adjacent cells are river cells would Eq. (7) be employed to calculate the river channel flux. A is the channel flow area [L²], and R represents the hydraulic radius [L]. Since the SGC model could be required to simulate relatively small, narrow, and deep channels, the model formulation was derived for the more general case in which the hydraulic radius of the channel is defined as the flow area divided by the wetted perimeter, instead of the h_{flow} in Eq. (4) that is designed for the shallow water flow (Neal et al., 2012). $Q_{c,\text{up}}$ is the upwind flow discharge [L³ T⁻¹]. Quite different from the floodplain flux calculation wherein the whole cell is used to transfer the

flux, the river channel discharge only occupies a proportion of a grid, depending on the ratio of the independently defined channel width to the cell dimension. The channel flow area quantifies the flow conveyance capacity as the product of the river width and flow depth. Overbank flow happens if the channel flow depth exceeds the bank elevation. Due to the deficiencies of typical bathymetry data and difficulties for field surveys to acquire continuous bathymetric information for flood inundation simulation, a simple method can be adopted for the estimation of the channel depth. By approximating the river channel as a rectangular geometry, the channel width and channel bed elevation can be estimated either as a function of the upstream discharge using empirical relations or gradually varied flow theory (Leopold and Maddock, 1953; Neal et al., 2021). The reason a rectangular river channel is applied for river hydraulics calculation is that the river width and depth are much more easily acquired compared with other parameters like the bottom width for a trapezoidal channel. The rectangular river channel allows the river bathymetry to be estimated in a way that is consistent with the observations, with an area equal to the surveyed cross-sections. It would be possible to code a more complex channel shape assumption should the application require it, and there is no fundamental reason why the channel must be rectangular beyond ease of parameterization and simplicity of the computation. Approximated channel features provide a feasible solution for simulating river hydraulics over regional- to continental-scale domains and in data-sparse areas. Externally specified bathymetry either from field surveys or some form of estimation process is also applicable if available.

Special attention should be paid to determining the upwind surface flux in the river channel. As depicted in Fig. 1, the cells with green represent the subgrid cells wherein the channel width is narrower than the grid dimension. For simplicity a uniform river width is applied for subgrid cells. The discharge is defined as positive if the flow direction is from west to east or from north to south. To calculate the discharge $Q_{ci,j-1/2}$, a combination of the surface discharge $Q_{ci-1/2,j-1}$, $Q_{ci,j-3/2}$, and $Q_{ci+1/2,j-1}$ is utilized if $Q_{ci,j-1/2} > 0$, which flows from north to south for the local cell surface flux (Eq. 8). While if the discharge $Q_{ci,j-1/2} < 0$, the flow propagation information comes from $Q_{ci-1/2,j}$, $Q_{ci,j+1/2}$, and $Q_{ci+1/2,j}$, which is the opposite flow propagation direction (Eq. 9). Hence, the upwind flow discharge is determined by judging the sign of the local cell surface discharge. Quite different from the 2D base model, which is decoupled in the x and y direction with upwind flow information coming from either the horizontal or longitudinal direction, the river channel should combine all the possible upwind flow discharge, though only one upwind flow discharge is in effect (the interface flux is not zero) for a single channel without a river confluence, as shown in Fig. 1b. At river confluences, discharge variation in three upwind surfaces is re-

sponsible for mass balance there, and all the possible sources of upwind surface flux should be considered (Fig. 1a).

Depending on the sign of the local interface flux, Q_{cup} , which represents the source of the flow information, is selected. The sign of each item in Eqs. (8) and (9) is dependent on the positive definition of river flow direction. In fact, $Q_{ci-1/2,j-1}$ and $Q_{ci+1/2,j-1}$ in Eq. (8) are zero as no river discharge exchange exists through these two interfaces (Fig. 1a). An extra minus sign is added to the right-hand side of Eq. (9) to coincide with local interface flux wherein $Q_{ci,j-1/2} < 0$ to ensure that the upwind flow information is not contradicted with the local flow status.

$$Q_{cup} = Q_{ci-1/2,j-1} + Q_{ci,j-3/2} - Q_{ci+1/2,j-1}, \text{ if } Q_{ci,j-1/2} > 0 \tag{8}$$

$$Q_{cup} = -(Q_{ci-1/2,j} - Q_{ci,j+1/2} - Q_{ci+1/2,j}), \text{ if } Q_{ci,j-1/2} < 0 \tag{9}$$

It is also noteworthy that upwind flow may still have a different direction to the local flow following Eqs. (8) and (9). For example, all four interface fluxes leave the current cell if there is a point source inside the cell, and the flow propagation direction is from the current cell to its four neighbour cells. Under such a situation it is apparent that all the interface fluxes have a unique flow direction, and no upwind flow propagation information is available for the four interfaces. Hence, further confinement is implemented to avoid the abuse of the contradicted upwind flow information (Eq. 10), or the upwind discharge would induce an unsteady flow condition, making the solution divergent. This constraint also applies to the floodplain momentum flux calculation. In fact, the numerical solution returns to the scheme employed in the original SGC model under such circumstances.

$$Q_{cup} = 0 \text{ and } \theta = 1.0, \text{ if } Q_{ci,j-1/2} \times Q_{cup} < 0 \tag{10}$$

Following the aforementioned procedures, wave propagation in the river and flood inundation over the floodplain can be calculated independently. No water exchange between the river channel and the floodplain exists at this stage. The interaction of flow information between the river and floodplain is accomplished inside the subgrid cells, as shown in the following section.

2.4 Water exchange at the river–floodplain interface

Subgrid cells can be used to route the flood wave downstream with the river channel bathymetry, and the remaining proportion of the cell can be used for floodplain flow propagation once the bankfull depth is reached, as shown in Fig. 1. The floodplain proportion in a subgrid cell is utilized to conduct the momentum exchange with its neighbouring floodplain cells, while the river channel part connects the upstream and downstream river cells. As the floodplain components only

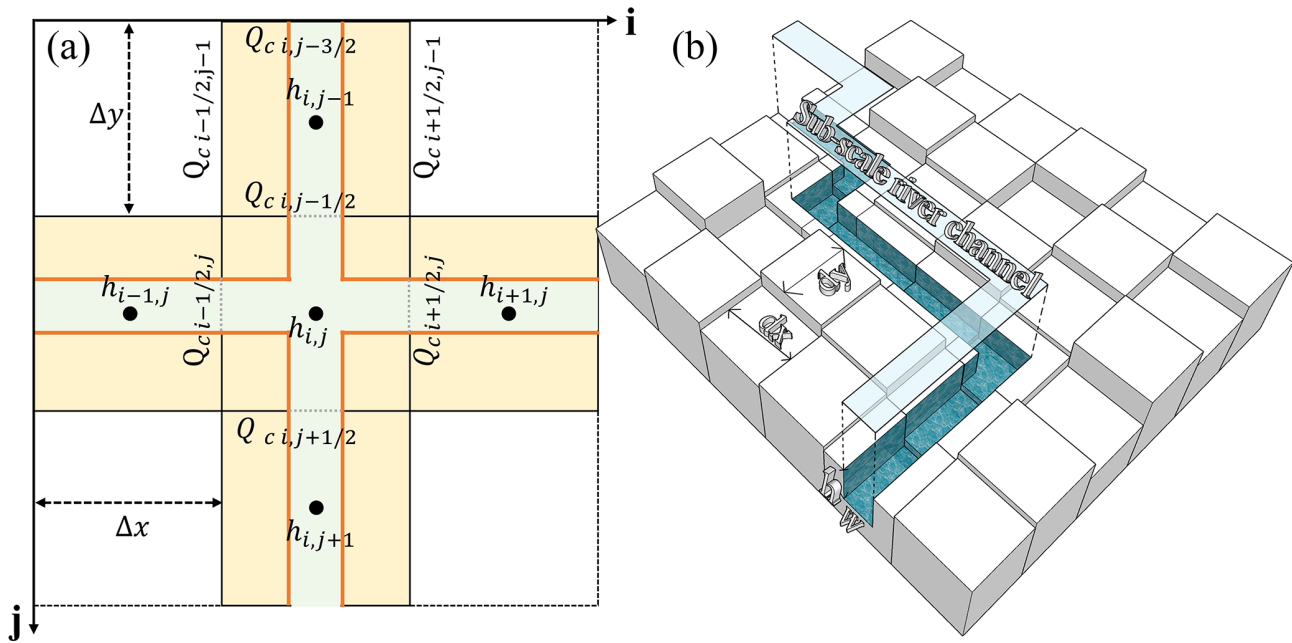


Figure 1. Subscale representation of the river channel on a coarse-resolution DEM. Subgrid cells are in shaded colours, with the black line showing the boundary of the DEM cells. Green shading represents the river channel, while the yellow shading represents the floodplain proportion with a subgrid cell. (a) A channel network with the river confluence. (b) A perspective view of a subscale river channel on the DEM grid.

take up a proportion of the subgrid cells, the capacity to transfer the momentum is to some extent reduced, depending on the proportion of the remaining width ($\Delta x - w_e$). The river channel and the floodplain component in a subgrid cell work together to update the water depth, and the same water surface elevation is shared by these two components when over-bank flow happens. Therefore, the water exchange is implicitly fulfilled without calculating the mass balance at the coupling interface to redistribute the water volume. Compared with a tricky treatment in the river–floodplain interface, the water exchange in the SGC model applies a simple storage cell that distributes the water volume explicitly. Momentum loss is neglected at the river–floodplain interface, and this is a reasonable critique of the scheme, but it is implemented for simplicity:

$$Q_{i-1/2,j}^{t+\Delta t} = \begin{cases} \frac{\theta Q_{i-1/2,j}^t + (1-\theta) Q_{i-3/2,j}^t - g \Delta t S_{i-1/2,j}^t h_{\text{flow}}^t (\Delta x - w_e)}{\left[1 + g \Delta t m_{i-1/2,j}^2 |Q_{i-1/2,j}^t| / \left[(h_{i-1/2,j}^t)^{4/3} A_{i-1/2,j}^t \right] \right]}, & \text{if } Q_{i-1/2,j}^t > 0, \\ \frac{\theta Q_{i-1/2,j}^t + (1-\theta) Q_{i+1/2,j}^t - g \Delta t S_{i-1/2,j}^t h_{\text{flow}}^t (\Delta x - w_e)}{\left[1 + g \Delta t m_{i-1/2,j}^2 |Q_{i-1/2,j}^t| / \left[(h_{i-1/2,j}^t)^{4/3} A_{i-1/2,j}^t \right] \right]}, & \text{if } Q_{i-1/2,j}^t < 0, \\ \frac{-g \Delta t S_{i-1/2,j}^t h_{\text{flow}}^t (\Delta x - w_e)}{\left[1 + g \Delta t m_{i-1/2,j}^2 |Q_{i-1/2,j}^t| / \left[(h_{i-1/2,j}^t)^{4/3} A_{i-1/2,j}^t \right] \right]}, & \text{if } Q_{i-1/2,j}^t = 0. \end{cases} \quad (11)$$

Here, w_e is the smaller channel width between two neighbour subgrids [L]. $(\Delta x - w_e)$ represents the remaining width perpendicular to the flow direction, which can be used to transfer the floodplain momentum. With the same governing equa-

tion for the river hydraulics and floodplain inundation calculations, the computational time steps in each component match each other, thereby increasing the robustness of the model. In every iteration, the coordinated time step is controlled by the Courant–Friedrichs–Lewy (CFL) condition to ensure the stability of the numerical scheme. The parameter α is included in Eq. (12) because the assumption of small amplitude in calculating the wave celerity is not always valid and because of the inclusion of friction terms in the model. The stable time step is therefore often somewhat less than that indicated by the CFL condition, so the parameter α is introduced to reduce the time step (Bates et al., 2010). The value of α is set to 0.7 for the simulations reported in this study, which is a trade-off between computational efficiency and numerical stability, but can be adjusted in the model by the user.

$$\Delta t = \alpha \frac{\Delta x}{\sqrt{gh_{\text{max}}}} \quad (12)$$

At every iteration, the time step is configured according to the maximum water depth over the domain. A predefined time step is utilized for the initial dry bed domain. At every time step, following the procedures mentioned above to update the flow discharge, the water depth in each grid is computed with Eq. (5). Considering the parsimonious demand for input data and the lower computational burden, the SGC model is a promising hydrodynamic model. In the next section, several tests are configured to evaluate the computational and numerical performance of the new SGC model.

3 Model testing and results

A structured sequence of numerical experiments that provide a rigorous test of the numerical and computational performance of the enhanced SGC model is configured. The accuracy and efficiency of the new SGC model are evaluated against the original SGC model (Neal et al., 2012), a first-order finite-volume (fv1) solver, and a second-order discontinuous Galerkin (dg2) solver (Shaw et al., 2021) within the same framework (LISFLOOD-FP). Realistic uncertainties over topographic errors and model system uncertainties can be compensated for by using the same code structure, thus making direct comparisons between the different techniques easier to achieve. All four solvers can be activated by assigning a separate parameter, which is very convenient for performing the calculation and comparisons. The original SGC model applied the solution scheme proposed by Bates et al. (2010) to discretize the local inertial equations. It has been reported that the scheme tends to break down for urban areas where the Manning values can be less than $0.03 \text{ m}^{-1/3} \text{ s}$. The fv1 solver is a first-order finite-volume method solving the integral form of full SWEs, and discontinuity in the solutions is captured by the HLLC approximate Riemann solver. The dg2 solver applies the discontinuous Galerkin method to solve the full-dynamic system (Kesserwani et al., 2018). A detailed description of these models can be accessed from this paper (Shaw et al., 2021). In principle, dg2 is the most mathematically accurate 2D hydrodynamic solver among the four, and a high computational cost is required to attain second-order accuracy. The main features of the four solvers are listed in Table 1. These models are set up to cover the potential theoretical limitations of the local inertial equations (de Almeida and Bates, 2013; Cozzolino et al., 2019), especially for areas where complex flow patterns are easy to form, involving rapidly varying supercritical flows, shock waves, or flows over very smooth surfaces.

The fv1 and dg2 solvers are full 2D hydrodynamic models without specially designed river-routing schemes. River hydrodynamics can be achieved with a high-resolution grid to include the predefined bathymetric features, with the channel width and depth data burned into the DEM in advance. Considering the variety of spatial discretization of fv1 and dg2 used, the first priority is to make sure that assimilation of the elevation data into each model leads to an identical representation of the site terrain. For an idealized test wherein river channel width is uniform, a high-resolution grid can be utilized to characterize the river channel, and the elevation data can be tailored manually before conducting the simulation to incorporate bathymetric information. Specifically, the strategy is to set the grid dimension identical to uniform river channel width and reduce the DEM elevation to the channel bottom for both the fv1 and dg2 solvers. For the remaining real-world tests, the limited grid resolution to identify the small-scale river channel because of the heavy computational burden makes it impossible to include the river bathymetry

in full 2D models. The fv1 and dg2 solvers are used here to provide inundation extent without considering the river hydrodynamics in order to analyse whether it is necessary to incorporate the subscale river component in flood modelling. In situ observation data are provided to benchmark the model performance. Specifically, these tests are as follows.

- Test 1: non-breaking wave run-up on a planar beach.
- Test 2: flow discharge distribution at a river junction.
- Test 3: subcritical flow over an undulating bed elevation in a rectangular channel.
- Test 4: simulation of flood propagation through a complex street and building network at a fine spatial resolution.
- Test 5: simulation of flood propagation in an integrated system with complex river channel network and floodplain topography.

Tests 1 and 3 are designed to explore the model stability and accuracy for a steady-state problem and an unsteady problem, respectively, each with an analytical solution or a well-approximated solution provided. Here the model ability for wave propagation in the river channel is assessed without considering the overland flow inundation process. The modelling performance at a river junction is assessed in Test 2 to validate the accuracy and robustness of the adaptive upwind solution scheme and assess how the scheme performs at distributary junctions. Test 4 is designed to test pure floodplain inundation over a complex urban area, with the emphasis on the assessment of the availability of the simplified model for the area where the complex flow pattern exists. The overall performance is assessed in Test 5, which involves the simultaneous calculation of river hydrodynamics and floodplain inundation process. Tests 1–3 were run on an Intel core i7-10850H eight-core CPU (2.70 GHz) with 16 GB of main memory and an OpenMP parallelization strategy, and Tests 4–5 were run on the University of Bristol high-performance computing (HPC) system with four nodes of a four-core processor with 64 GB of RAM per node. Previously, these tests were successfully used in practical applications. By conducting these tests, the model ability to simulate the wave propagation in the river channel, flood inundation over the floodplain, and water exchange over the river channel and floodplain boundaries is investigated. The model performance is assessed in terms of the RMSE, volume error, and total computational time.

3.1 Test 1: non-breaking wave run-up on a planar beach

The test developed by Hunter et al. (2005) aims to simulate the water flow running up a planar beach as the upstream water depth rises slowly. No analytical solution exists but

Table 1. Main features of solvers in the LISFLOOD-FP model.

| Model | Equations | Shock capturing | Time step and stability | Computational efficiency | Accuracy | Disadvantages |
|--------------|---------------------------------|--|---|--|--|---|
| Original SGC | Local inertial equations | Shocks are not represented by the governing equations. | $\Delta t = \alpha \frac{\Delta x}{\sqrt{gh_{\max}}}$, unconditionally stable | High efficiency based on OpenMP. | Well-approximated for subcritical and gradually varied flow. | The scheme tends to be unstable for urban areas ($n < 0.03$). |
| Improved SGC | Full 2D shallow water equations | The shocks are captured by Godunov's method. | $\Delta t = \alpha \frac{\Delta x}{ u + \sqrt{gh_{\max}}}$, unconditionally stable with $0 < \alpha < 0.33$. | A high computational cost is required. | The most accurate solver theoretically. | The scheme may overestimate the water depth near the wave front for high friction ($n > 0.06$). |
| fv1 | | | | | Less accurate | Fv1 solver would in general overestimate the water depth. |
| dg2 | | | | | | Time-consuming. A small time step is demanded. |

a well-approximated numerical solution can be acquired by the fourth-order Runge–Kutta method and taken as the reference solution. The planar beach with an adverse slope of $1/6000$ is configured with a wide range of friction parameters ($0.01, 0.03$, and $0.06 \text{ m}^{-1/3} \text{ s}$) to check if the new SGC model can provide stable solutions, especially for low-friction areas where the original SGC code is prone to collapse. The flow speed is $u = 1 \text{ m s}^{-1}$, mesh resolution is 50 m , and the total simulation time is 5000 s . The test reveals key details about the fundamental capabilities of the solvers in simulating the propagation of flood waves across initially dry sloping beds.

All four solvers run efficiently for the planar beach test with such a simple topography and boundary conditions, and the results are all acquired within 1 min , most of which are fixed computing costs such as I/O and array initialization. The dominant wave propagation characteristics on the initially dry bed sloping planar can be captured by all four solvers. Considering the accuracy of the four solvers, the dg2 solver based on the full SWEs has the best approximation to the reference solution, while an overestimation of the water depth is captured by the fv1 solver in all three scenarios (Figs. 2 and 3). Even though the fv1 solver is constructed on a full-dynamic shallow water system, it does not perform as well as the improved SGC model based on the local inertial equations. A possible reason why the fv1 solver has

an unsatisfactory performance is that the first-order finite-volume approximation cannot keep all the necessary flow information due to the truncation error, and the solver can be severely affected by rapid accumulation of numerical diffusion, particularly when the fine resolution needed to alleviate these errors is unaffordable (Ayog et al., 2021). The two SGC solvers have some of the properties of a second-order scheme as a result of the staggered grid and therefore avoid this issue. While the dg2 solver based on the full-dynamic SWEs is preferred here due to its high accuracy, an efficient solver based on the simplified version of the governing equations that retains the dominant hydraulic features of the flow field would be favoured for many practical applications. The improved SGC model appears to be a promising solver with less computational resource demand than dg2 considering that the maximum volume error in all three scenarios is -0.5% .

As depicted in Fig. 2a, the original SGC scheme deviates from the others as expected at $n = 0.01 \text{ m}^{-1/3} \text{ s}$, while the improved SGC model with the upwind solution scheme is still accurate at this friction. The fluctuation in the water elevation profile at low friction also implies that the original SGC scheme has broken down and become unstable. A tendency to deviate from the analytical solution can be found under $n = 0.03 \text{ m}^{-1/3} \text{ s}$ (Fig. 2b); the original SGC model has a slow wave speed (17% slower than the analytical solu-

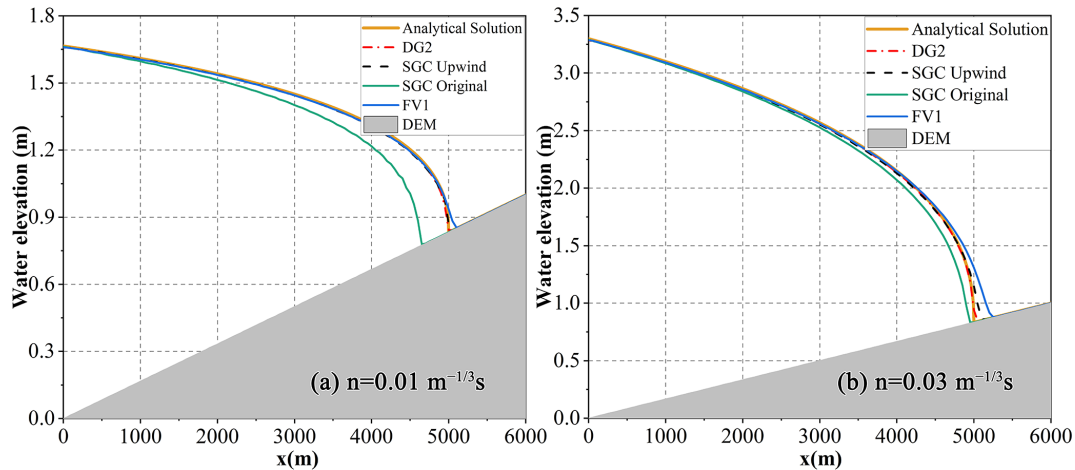


Figure 2. The water elevation profile calculated by the four solvers (dg2, fv1, original SGC, and improved SGC) under $n = 0.01$ and $0.03 \text{ m}^{-1/3} \text{ s}$ at $t = 5000 \text{ s}$.

tion near the wave front), and the predicted water depth follows behind the analytical solutions. The difference grows as the friction parameter is progressively reduced, and eventually the original scheme diverged, resulting in a 279 m lag at the wave front after 5000 m of wave travel. After implementing the upwind-solution-sensitive stencil, the artificial diffusion that corresponds to the direction of flow information propagation is included, and a more robust and accurate stencil is formulated. The new SGC model outperforms the original SGC model, and the volume error and the RMSE from the analytical solution also evidence the better performance of the improved SGC model (Table 2).

The new SGC model does not always have a better performance than the original scheme over the whole domain. For the simulation with a high friction parameter ($n = 0.06 \text{ m}^{-1/3} \text{ s}$), a slight overestimate of the water depth is found near the wave front for the improved SGC model, shown in Fig. 3. Even with the divergence near the wave front, RMSE for the improved SGC model is still only 0.07 m. For many applications this is probably acceptable as this is less than the vertical error in typically available terrain data (Bates et al., 2010). Considering the overall performance of all the solvers, the new SGC solver indeed improved the stability and accuracy of the original scheme, especially for the low-friction case.

Table 2 shows the volume error and the RMSE of the water elevation from the analytical solution of the four solvers under different friction scenarios. A sufficiently physical description of the wave run-up on an adverse slope is captured by the dg2 solver, and the predicted water depth is a good approximation of the analytical solution, with a maximum RMSE of 0.037 m and maximum volume error of -0.48% in all three scenarios. The total volume of water in the domain is error-free even after a long time evolution of the full-dynamic system. The improved SGC model shows a performance

comparable to the dg2 solver, with a maximum RMSE of 0.072 m. The original SGC and the fv1 solver are more sensitive to friction parameters. An obvious underestimation of the water depth is witnessed at $n = 0.01 \text{ m}^{-1/3} \text{ s}$ for the original SGC with a maximum volume error of -6.26% , while a significant overestimation of the predicted water depth is observed for the fv1 solver with maximum RMSE of 0.174 m. The fluctuations in model performance for the original SGC and fv1 solver indicates that the solution method is of vital significance compared with the different versions of the governing equations. Given the overall performance of the improved SGC model, we can confirm that the upwind-form stencil with adaptive artificial diffusion enhances the model stability and accuracy over the original SGC scheme.

3.2 Test 2: flow discharge distribution at a river junction

A reasonable approximation of the flow discharge distribution at a river confluence is of vital importance for river hydraulics modelling in many situations. Modelling performance in a single river channel is validated in Test 1, while the reliability and the accuracy of the new solution scheme at a river confluence have not been evaluated in any previous research, and little is known about how the scheme performs at tributary junctions. Test 2 is therefore configured to assess the robustness of the new river hydraulics solution scheme in this situation. A total of three cases with different arrangements of a rectangular river channel, ranging from simple to complex, are set up for evaluation of the river hydraulics solution strategy. As shown in Fig. 4a, a sloping rectangular river channel with a fixed water head of 0.1 m (i.e. steady-state conditions) is set up, with a slope of 1/1000 and a uniform Manning parameter of $0.06 \text{ m}^{-1/3} \text{ s}$. The same configuration also applies to case (b) and (c). Case (b) combines two identical rectangular river channels, intersecting at the mid-

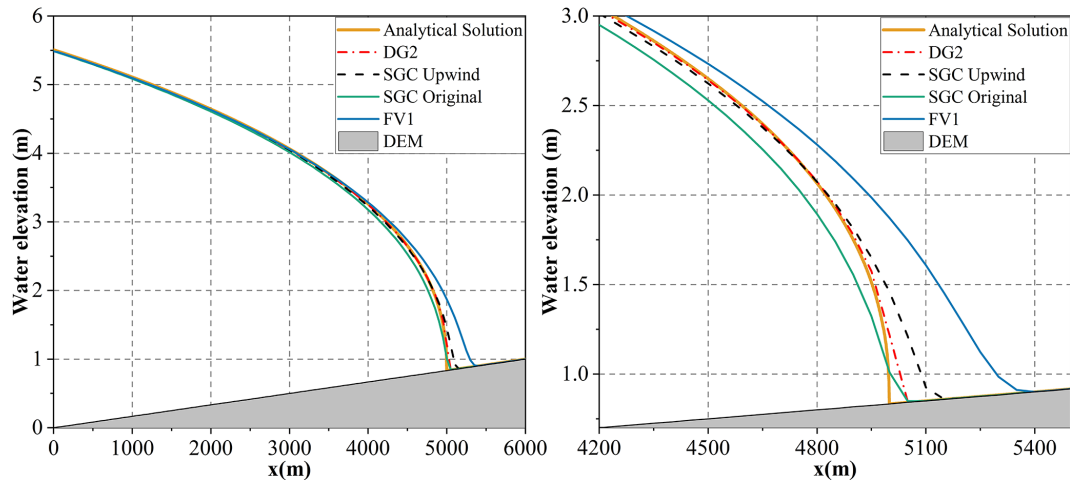


Figure 3. The water elevation profile calculated by the four solvers (dg2, fv1, original SGC, and improved SGC) under $n = 0.06 \text{ m}^{-1/3} \text{ s}$ at $t = 5000 \text{ s}$ and an enlarged view at the waterfront.

Table 2. Impact of the friction parameter on water elevation RMSE and volume error.

| | $n = 0.01$ | | $n = 0.03$ | | $n = 0.06$ | |
|--------------|------------|------------------|------------|------------------|------------|------------------|
| | RMSE (m) | Volume error (%) | RMSE (m) | Volume error (%) | RMSE (m) | Volume error (%) |
| dg2 | 0.006 | -0.48 | 0.013 | -0.11 | 0.037 | -0.20 |
| Improved SGC | 0.007 | -0.51 | 0.035 | -0.36 | 0.072 | -0.39 |
| Original SGC | 0.094 | -6.26 | 0.078 | -2.52 | 0.066 | -0.32 |
| fv1 | 0.011 | -0.67 | 0.067 | 0.960 | 0.174 | 1.58 |

point of these two channels. River flow with the same water depth boundary condition as in case (a) in these two tributaries runs down at a planar slope and joins at the river junction cell, and the intersection cell plays the role of balancing the discharge allocations for the two downstream tributaries. As the modelling accuracy in the river channel has been validated in Test 1, case (a) is taken as a reference for the validation of the solution accuracy at a river confluence, and no analytical solution is provided. Case (c) is configured to evaluate the discharge distribution at a river junction, where water is continuously supplied from one main stream. All the river channels are surrounded with a bank that is sufficiently high to avoid water exchange at the river–floodplain interface.

For the calculation of the local cell surface flux at one boundary of a river confluence grid, the other three grid boundaries may be included, depending on the local flow direction, as all flux exchanges with the confluence cell are responsible for the mass balance there (Eqs. 8 and 9). The water depth profiles for these three cases at $t = 131 \text{ s}$ are shown in Fig. 5, representing a transient flow status before reaching a steady-state solution, which is a common water depth profile in this situation. A similar slight overestimation of the water depth near the wave front as in Test 1 was found for the upwind solution scheme (blue line) in case (a), with a Manning

parameter of $0.06 \text{ m}^{-1/3} \text{ s}$. An identical water depth profile is calculated for the two downstream tributaries in case (b), marked as a purple line and black line with small circles in Fig. 5, which guarantees that an identical treatment is applied to the horizontal and vertical flow movement in the new upwind solution schemes. The nearly identical water depths in cases (a) and (b) confirm that an acceptable performance has been achieved with the new scheme. The slight overestimation of the water depth in case (b) is influenced by the intersection of the two streams. When the two streams join at the river junction cell, we have twice the discharge entering the cell without quite twice the cell area. The water volume at the intersection cell increases and a higher water depth gradient can be expected for the two downstream tributaries. Therefore, a greater flow velocity exists due to the large water elevation gradient, resulting in an expected overestimation of the water depth profile compared with the single river channel case. Case (c) demonstrates the discharge distribution for three downstream tributaries. A symmetrical water depth profile in the y direction (purple line), which is the same as the water depth in the x direction (blue circle), is acquired, implying that the discharge is evenly allocated among the three tributaries. Inclusion of all upwind exchange, which may have a potential impact on the mass balance at a river junction cell, guarantees the identical treat-

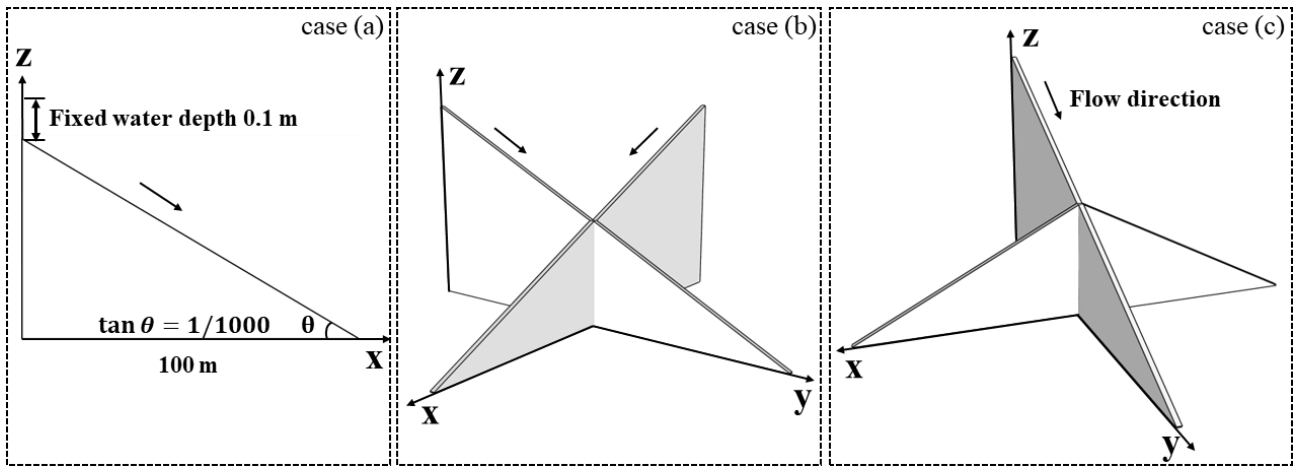


Figure 4. Validation of the new solution strategy at a river junction with different arrangements of a sloping rectangular river channel. (a) A single river channel. (b) Two identical sloping channels intersecting at a junction cell. (c) A main stream provides flow for the same three downstream channels.

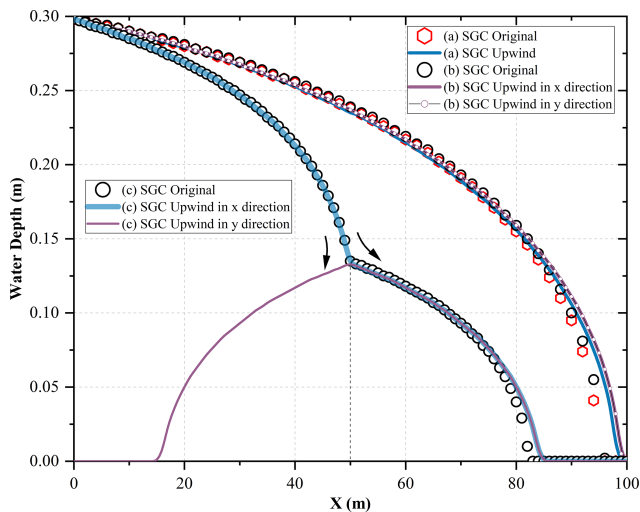


Figure 5. Water depth profile predicted by the two SGC solvers at $t = 131$ s. Panel (a) shows the water depth predicted by a single sloping river channel, panel (b) shows the two channels intersecting at a confluence, and panel (c) shows the flow distribution from a main stream to three downstream channels.

ment of these downstream tributaries. If only one upwind discharge in the same direction is considered, water depth in the x direction can always be higher than the y direction as no upwind discharge exists for the flow in the y direction at the intersection of these three tributaries. Assuming that no energy loss is generated when flow direction changes, the new upwind solution schemes keep a balance between the mass storage and the momentum exchange at a river confluence, making sure that the flow movement can be accomplished in a simplified way.

3.3 Test 3: subcritical flow over an undulating bed elevation in a rectangular channel

Test 3 is derived from de Almeida and Bates (2013) and explores a steady flow regime in a 5 km long and 10 m wide rectangular channel with a Manning coefficient of $0.03 \text{ m}^{-1/3} \text{ s}$ (a 1 km long river is also configured). The upstream discharge is set to $2 \text{ m}^3 \text{ s}^{-1}$ and the downstream water elevation is determined according to Eq. (14). To derive the analytical solutions of the steady flow regime, a subtle approach is used for the inverse problem. Given the water elevation profile and boundary conditions, the bed elevation that we seek is acquired by integrating the channel slope analytically derived from the steady flow form of the Saint-Venant equations. This test provides a rigorous assessment of the model’s ability to accurately simulate a range of steady-state flow conditions.

$$S_0 = \left[1 - \frac{4}{gh(x)^3} \right] h'(x) + \frac{0.0036}{h(x)^{10/3}} \tag{13}$$

$$h(x) = \frac{9}{8} + \frac{1}{4} \sin\left(\frac{\pi x}{500}\right) \tag{14}$$

$$h'(x) = \frac{\pi}{2000} \cos\left(\frac{\pi x}{500}\right) \tag{15}$$

Here, $h(x)$ is the water depth profile and $h'(x)$ its spatial derivative, and S_0 is the channel slope. Following Eqs. (13)–(15), the analytical solution of the water depth and channel bed elevation for the 5 km long channel is formulated. Due to the advection term being ignored in the local inertial equations, the side effect of the simplified local inertial equations is considered to attenuate any oscillations of the water depth (de Almeida and Bates, 2013). Therefore, the 1 km long channel is configured to introduce a more oscillating channel bed elevation, investigating the applicability of the local inertial equations for a high-oscillation environ-

ment. To set up the analytical solution for the 1 km channel, the wavelength in Eq. (14) is reduced by a factor of 5 while the wave number remains unchanged, and thus the oscillation frequency increases. The water depth gradient is computed by differentiating Eq. (14). After substituting Eqs. (14) and (15) into Eq. (13), the slope along the river channel is determined, and the channel profile is calculated by further integrating the slope using high-resolution quadrature methods. More simply, the 1 km long channel is achieved by compressing the x axis of the 5 km long channel, whilst the wave amplitude remains unchanged. A comparison of the analytical solution with the water depth and channel bed elevation calculated by the different solvers is shown in Fig. 6a. The predicted water depth from all four solvers agrees well with the analytical solution at the final steady state, with maximum RMSE of 0.021 m. The water oscillates at a high frequency in the 1 km long channel, and a highly oscillatory water depth profile is therefore created. However, an opposite trend is witnessed in Fig. 6b for solvers based on the full SWEs (fv1 and dg2) and the local inertial equations (SGC solvers) as we reduce the channel length.

As is depicted in Fig. 6b and c, the water depth predicted by the local inertial equations is lower than the full-dynamic SWEs for subcritical flow, indicating that the SGC model indeed attenuates some oscillations in the water depth. As we decrease the channel length and naturally increase the frequency of the channel bed oscillation, an increased departure from the solution is obtained for models based on the different governing equations. Owing to the impact of the non-linearity in the friction term, a larger energy loss is included for the highly oscillatory depth profile. As a consequence, a further underestimation of the water depth is found in the SGC model for the 1 km long channel. Originating from the intrinsic characteristics of the governing equations wherein the advection term is ignored, the discretization method cannot change the final behaviour of the steady-state problem. At last, the water depth calculated by the two SGC solvers shares the same water depth profile, even though they are different before the formulation of the steady state. For the fv1 and dg2 solvers, the highly oscillatory depth profile is also accompanied by greater energy losses without the attenuation of the flow depth gradient. The water depth is retained by the full-dynamic system, and a high-fluctuation water depth profile is well-captured by the solvers based on the full-dynamic system. However, the disparity is relatively small (0.07 m) compared to even the best wide-area terrain data (i.e. airborne laser altimetry or lidar), indicating that the SGC model based on the local inertial equations could still be used for a wide range of steady-state problems.

It takes about 2 min for the SGC model to achieve the steady-state water depth profile for $L = 5000$ m, which is 5 times faster than the dg2 solver and 2 times faster than the fv1 solver. Considering the lower computational resources required while still preserving spatially second-order accurate results that are close to the dg2 solver given typical real-

world errors, the SGC solver would be a promising alternative, especially for large-scale flood modelling. From the perspective of model accuracy, all numerical results show excellent agreement with the analytical solution when they reach steady state. However, it has been noticed that the original scheme struggles to keep a stable state, and divergence of the original SGC scheme is captured before reaching the final steady state, even though a high-resolution 1 m grid is adopted. For the improved SGC model, no obvious divergence is captured during the formulation process of the steady state. By implementing the improved numerical scheme in the SGC model, the potential instability problem can be eliminated, enabling the achievement of a reliable result more easily.

The adaptive weighting factor θ in Eq. (6) has a minimum value of 0.3, provided that the α in Eq. (12) is 0.7. Statistics of the distribution of θ acquired during the calculation process indicate that $\sim 92\%$ ranges from 0.70 to 0.83, so only at the very early beginning of the simulation can θ be less than 0.7. After reaching a steady state, nearly all θ remains within 0.70–0.83. Tests 1 and 2 also demonstrated that θ can be smaller than 0.7 only in very rare conditions. Therefore, an extra constraint is adopted, which allows θ to vary from 0.7 to 1.0. A similar strategy has also been implemented in Sridharan et al. (2021). By limiting the minimum value of θ to 0.7, a limited impact of upwind flow information can be applied, which makes sure that the local flow status can always dominate the local discharge update. Without such a constraint, the dominant upwind flow discharge can always accelerate the flow speed, and too much dependence on the upwind flow information while ignoring the local flow status can easily cause mass balance error.

3.4 Test 4: fine-resolution flood propagation over the complex urban environment

Tests 1–3 are idealized cases that assess the accuracy and stability of the improved SGC model against analytical solutions. However, the model ability and efficiency for modelling river–floodplain systems have not yet been evaluated. The following tests are configured to test the simulation of real-world flood propagation process to thoroughly check the model performance. Test 3 is motivated by Hunter et al. (2008) and is applied to investigate the model ability to simulate flood propagation over complex topography. The domain covers an area of 1000 m by 400 m in the city of Glasgow, Scotland, with dense urban development along both sides of the two main streets at the site and a topologically dense network of minor roads, as shown in Fig. 7. A flash flood event with rapid hydrograph rise and fall that occurred on 30 July 2002 is simulated. A 1 m resolution lidar DEM is filtered to remove the buildings and vegetation to give a “bare earth” DEM that includes some steep stretches of road and isolated depressions where water may accumulate. The DEM has a horizontal and vertical accuracy of less

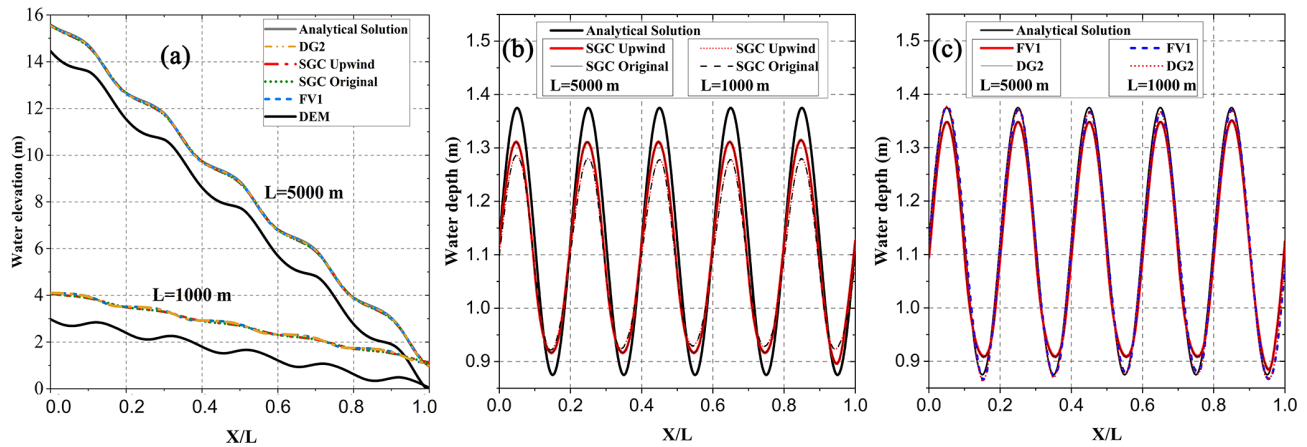


Figure 6. Water depth profile predicted by four solvers under $L = 1000$ m and $L = 5000$ m. (a) Water elevation and the river channel bed elevation profiles. (b) Water depth predicted by two SGC solvers under different oscillating frequencies. (c) Water depth predicted by the fv1 and dg2 solvers.

than 50 and 15 cm RMSE, respectively, and is further fused with the Ordnance Survey OpenData (<https://osdatahub.os.uk/downloads/open>, last access: 31 May 2023) to identify the location of the buildings. The cells wherein the buildings are located are raised in elevation by 6 m to represent an arbitrary building height, as shown in Fig. 5. A point source inflow boundary condition with the same hydrograph as in Hunter et al. (2008) is established at location P0, and other boundary conditions are set to closed since there is no mass flux interaction at these boundaries. The flash flood lasts about 1 h, and a simulation period of up to 5 h is conducted to allow the water to come to rest and pond in depressions. A simple calibration process is performed for the selection of optimized roughness coefficients. Taking the water depth distribution from Hunter et al. (2008) as the reference, different pairs of roughness coefficients chosen from a wide but physically plausible range were set up to mimic the effect of typical calibration procedures. The Manning roughness for smooth streets varied from 0.01 to 0.03, while for other areas it varied from 0.01 to 0.08, both in steps of 0.005. This results in an optimized Manning's roughness for smooth streets of 0.02, while other areas have roughness coefficients of $0.05 \text{ m}^{-1/3} \text{ s}$, where the calculated water depth distribution has a hit rate of 0.99 compared with the reference.

Figure 7 illustrates the predicted water depth distribution of the dg2 and improved SGC solvers. A similar flood inundation extent is obtained by these two solvers, while the dg2 predicted a later recession of the flood propagation. The interaction with the building configuration and convergence in low-lying regions characterizes the complex flow field. Flow is thus a complicated combination of high-velocity shallow flow and ponding in low-lying regions. The complex flow patterns (e.g. numerous transitions to supercritical flow, numerical shocks, and flows over very smooth surfaces) in the urban environment pose significant challenges for an accu-

rate representation of the flood inundation process. As we can expect, the SGC model cannot capture all the hydrodynamic features in such an environment while only retaining the dominant factors impacting the flood propagation (pressure, friction, and local acceleration). However, the improved SGC model is found to provide a reasonable approximation of the full-dynamic SWE solvers considering the water depth distribution. At peak inundation, the mass error is comparable to a height error of only 3.5 mm when dispersed across the whole inundated region. When it comes to the computational efficiency, the dg2 solver and fv1 solver have an increase in the simulation time compared with the SGC model. The SGC solver acquires the final results within 2 min, which is 4 times and 6 times faster than the fv1 and dg2 solvers, respectively.

Owing to the lack of in situ observation data, results calculated by the dg2 solver are taken as the benchmark. The at least second-order-accurate dg2 solver can acquire more details impacting the hydrodynamic processes, leading to a more complete water depth distribution. Figure 8 shows the maximum absolute error distribution of the fv1 and SGC solvers compared with the dg2. Considering that all of the absolute errors are within the range 0.1 m, the specific error value is omitted, and only the three categories characterizing the maximum deviation from the dg2 results at each DEM cell are depicted. 57 % of the area is occupied by red, which indicates that the water depth difference between the original SGC solver and the dg2 is the largest. In the southern part of the domain where the low-lying regions suffer from severe flood damage, the fv1 solver gives the largest overestimation of water depth (relative to dg2), with the areas where fv1 is maximal occupying 39 % of the whole inundation area. The improved SGC solver yields well-approximated results compared with the dg2 solver, and only 4 % of the inundation extent shows an obvious deviation from the dg2. One possible



Figure 7. Flood inundation extent at $t = 4200$ s calculated by (a) the dg2 solver and (b) the improved SGC solver. Background maps in (a) are © Google Maps screenshots.

reason why the new SGC solver can improve the model accuracy compared to the original SGC scheme is that the latter will break down in such an urban environment, especially for areas with a combination of a small Manning value and shallow water depth. The implementation of the upwind scheme together with the adaptive weighting factor alleviates the tendency of divergence. The improved SGC solver predicted a slightly larger inundation extent near P0, illustrating a rapid ponding area at the start of the simulation, followed by a gradual release of water as the simulation progresses. The upwind water depth is always higher here, and the upwind scheme would predict a slightly larger surface flux compared with the scheme adopted in the original SGC solver. Thus, the flow can march further at the wet–dry boundary, and a broader inundation extent exists. In other areas of the domain the different flow tributaries and the interaction with

the buildings induce a varying flow field. As a result, the predicted surface flux from the new SGC solvers approaches the true flux as a result of the adaptive weighting factor. The proposed SGC model (only the floodplain component as no channel is included in this test) can provide oscillation-free solutions even on smooth surfaces in urban areas and exhibits good agreement with dg2 in most locations without the need for trial-and-error modification of the value of the diffusion coefficient.

Figure 9 depicts the time series of water depth variation at the four points shown in Fig. 7. P1 is monitoring the water depth variation on the street close to the water inlet. The relatively smooth street transfers the flood wave downstream quickly without holding back the water volume. The shallow water begins to divide into several branches as the flow proceeds further into the domain. The original SGC solver pre-



Figure 8. Maximum water elevation difference of the fv1 and SGC solvers compared with dg2. Background vector data are © Ordnance Survey OpenData.

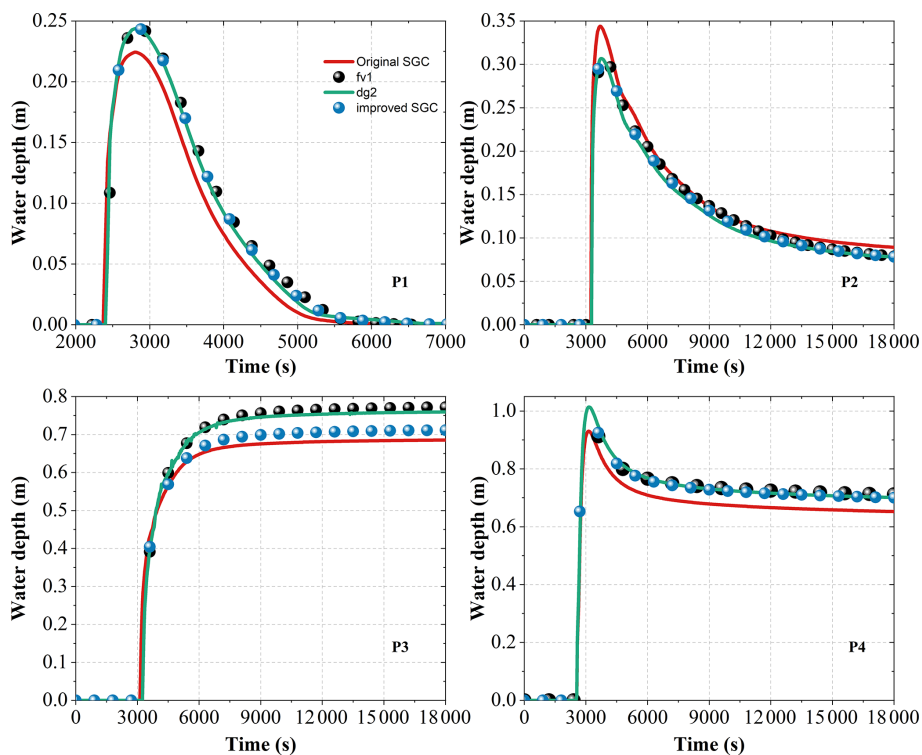


Figure 9. Time series of water depth variation in four locations: P1–P4 (locations of P1–P4 are shown in Fig. 7).

dicts an early arrival of the flood peak, together with a quick recession as the simulation proceeds. The maximum deviation of the flood peak is 0.169 m, and the water depth predicted by the other three solvers is in good agreement. Data from P2 show that the original SGC solver attenuates the water amplitude as the flow is shallow and has high-velocity

status on the street. A slight overestimation of the flood peak compared to the others is captured by this solver, and the discrepancies are about 4 cm, which is of the same order as the vertical error in the lidar DEM (RMSE of ~ 5 cm). P4 is an area where the flow interacts with buildings, and the combination of shallow water depth and the flow around build-

ing blocks leads to a complex flow status. As a result, the RMSE between the original SGC and dg2 is ~ 5 cm, while a 1.5 cm RMSE is given for the improved SGC solver. Complex flow patterns also exist near P3. The high-speed shallow water from both sides of the street merges, forming a deep low-velocity flow field. The constraints imposed by the buildings on both sides of the street influence the flow propagation direction, which further aggravates flow oscillations. Therefore, a large volume of water converges here, leading to higher water depth and obvious water depth differences. However, the maximum water depth difference is limited to within 0.1 m. The original SGC solver still has the maximum deviation from dg2, with a maximum RMSE of ~ 6 cm, while the new SGC solver has an RMSE of ~ 3.5 cm. Overall, the improved SGC model can generate oscillation-free solutions even on smooth surfaces in urban areas and shows good agreement at all stations with a full shallow water second-order model.

3.5 Test 5: simulation of flood propagation in an integrated system with complex river channel network and floodplain topography

Test 5 reproduces a flood inundation process in the Carlisle 2005 urban flood event caused by heavy rainfall. Over a 36 h period preceding the flooding, up to 175 mm of rain fell over the Eden catchment in which the city of Carlisle sits. Overflow from the River Eden and backwater flow impacts along the rivers Caldew and Petteiril aggravated a severe situation and led to considerable flood damage. Overall performance of the improved SGC model is assessed in Test 5, and the modelling capacity to represent wave propagation in a river channel with floodplain inundation dynamics and water exchange at the river–floodplain interface are evaluated with the real-world test.

The underlying topography is constructed with a combination of lidar fused with digital map data. Lidar data with the estimated RMSE of 0.197 m are provided by the Environment Agency of England and Wales, as are the cross-section data with an interval of 200 m on the River Eden and 50 m along the rivers Petteiril and Caldew. Vegetation is removed from the source data while the building information is retained, and thus a 10 m resolution DEM with a vertical RMSE of 0.38 m and a mean error of 0.07 m is acquired. Cross-section data are further interpolated to approximate the river bathymetry, with the river channel being “burnt” into the DEM. The resultant topography data with a resolution of 5 m are collected from Horritt et al. (2010). Due to the relatively high runtime cost, the finest 5 m DEM is resampled to 10 m and a total of ~ 146 thousand grids are generated. Both fv1 and dg2 are pure 2D models and therefore represent the channel and floodplain as a continuous unit, and these models are therefore applied directly to the 10 m DEM with “burnt-in” rivers. In contrast, the SGC model applied a separately configured river channel bathymetry for the river

hydraulics calculation, and the 10 m DEM is applied for the flood modelling, to ensure that all values inside the SGC output stencil are equivalent to the fv1 and dg2 model results with no averaging or interpolation. The same time series discharge as in Neal et al. (2009) is taken as the inflow for the three rivers, and a free outlet boundary condition is imposed on the River Eden close to the Sheepmount gauging station. All flow is expected to enter and leave the model domain via these river channels. Two post-event surveys of the wrack and water marks were undertaken by the University of Bristol and the EA, and 183 point measurements of maximum water surface elevation were acquired and used for calibration of the Manning’s roughness values. A total of 78 simulations were conducted that form a matrix of 13 effective n values for the channel model (0.01, 0.02, 0.03, 0.035, 0.04, 0.045, 0.05, 0.055, 0.06, 0.065, 0.07, 0.075, and 0.08) and six effective n values for the floodplain model evenly spaced between 0.02 and 0.12. These ranges were deliberately large to ensure the optimum was bracketed. When simulated inundation extent did not reach a wrack or water mark, the water surface elevation of the nearest wet cell was used to calculate the simulation error. The pair of Manning’s roughness values for the floodplain and river channels which resulted in the smallest RMSE compared with the surveyed water marks was selected as the optimized roughness value. The optimized Manning parameter is $0.04 \text{ m}^{-1/3} \text{ s}$ for the channel and $0.06 \text{ m}^{-1/3} \text{ s}$ for the floodplain. Given that the major aim of the test is to evaluate the model performance, the model still employs the 2005 terrain and flood defence information even though new defences were constructed following the 2005 flood event.

The maximum flood inundation extent with the water depth distribution calculated by the improved SGC solver is depicted in Fig. 10. Many surrounding districts of Carlisle such as Willowholme, Caldewgate, Denton Holme, Botcherby, and Harraby Green are flooded, and this coincides with the observed flood inundation extent. The dark blue line with a water depth deeper than 6 m characterizes the locations of the three major rivers in the domain. Further analysis of the inundation propagation process confirmed that the river channel conveys a significant proportion of the flood volume, and at the end of the simulation 67 % of the flood volume was being routed downstream through the river channel at the outlet boundary. This test highlights the vital importance of in-channel hydraulics modelling even during out-of-bank floods. The modelling of flow conveyance capacity and estimation of mass and momentum exchange at the river–floodplain interface impact the inundation process significantly. Even with a 10 m DEM and full 2D model, the river channel wave propagation cannot be correctly represented in this case without an independent river hydraulics model, and a slightly different inundation process is obtained with fv1 and dg2 that has larger errors compared to the observed water level data. Floods in the full 2D hydrodynamics model may spread over the floodplain earlier than the SGC solvers, and

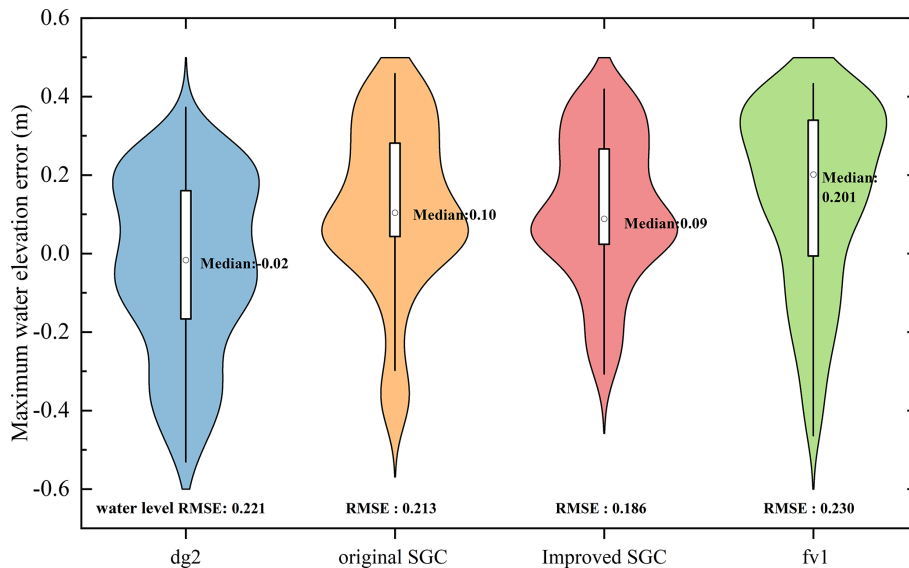


Figure 11. Water surface elevation errors of the four solvers compared with the field survey point data.

vital importance of river hydraulics modelling for simulating flood flows.

The final water depth distributions from the two SGC solvers are quite similar, and the maximum difference lies in the fact that the original SGC solver underestimates the water depth with a deviation from in situ data of -0.4 m. Most of these abnormal points are located at the edge of the inundated area. A possible explanation is that the adaptive artificial diffusion solution scheme can adjust the discharge automatically and responds more quickly to the upwind flow discharge variation, while the original solution scheme is impacted by the small friction and interaction with building blocks and suffers from a flood recession that is too quick as a result.

Keeping a balance between the modelling efficiency and the grid resolution is a major task for flood modelling, especially when small-scale river channel bathymetry controls the flooding process. Representing dominating river channel bathymetry features can inevitably increase the runtime of the full 2D hydrodynamic models, while ignoring these features cannot capture the dominant flood inundation process. The strict time step required for full 2D hydrodynamic model stability further limits the modelling efficiency. As a result, the dg2 solver takes more than 15 times the computational time of the SGC solver, while the fv1 is approximately 5.2 times slower than the SGC solver. The SGC model with the improved modelling stability in urban environment provides a powerful alternative there, which preserves the small-scale river channel features while keeping a high efficiency. With the support of the improved SGC model, the model accuracy can be increased to a useful extent. In particular, abnormal water depth distributions can be removed with the adaptive artificial diffusion solution scheme. The improved

SGC model therefore provides a better alternative for the river–floodplain inundation simulation.

4 Discussion and conclusions

The SGC model, which allows utilization of approximated subscale bathymetry while performing computations on relatively coarse grids, has been extensively applied to track the wetting and drying dynamics in the river–floodplain system. Based on the simplified efficient inertial formulation of the shallow water equations, the SGC model provides a feasible solution for large-scale flood modelling. However, the solution scheme of local inertial equations in the original SGC model suffers from numerical instability in the case of low-friction scenarios. Many measures have been proposed to improve the accuracy and robustness of the solutions. Unfortunately, the SGC model to date has not included these latest developments in numerical solutions of the local inertial equations. In this paper, for the first time we implement a previously developed artificial diffusion and explicit adaptive weighting factor in the SGC model. Compared with the original solution stencil, the new solution scheme explicitly includes the artificial diffusion in the form of an upwind scheme to improve the estimation of the numerical flux, and the automatic recognition of the diffusion needed to stabilize the solution stencil is achieved with an adaptive procedure based on the local flow status. A further constraint is adopted in this paper to limit the amount of artificial diffusion, which demands that the adaptive weighting factor varies from 0.7 to 1. Momentum exchange is always dominated by the previous local surface flux, while limited artificial diffusion in the form of upwind surface flux is included to avoid mass balance errors by this mean. Evaluation of the new SGC model

through a structured test, from simple river hydraulics calculation to a real-world flood inundation simulation, confirmed that accurate mass and momentum balance in shallow flows over complex geometries is ensured in the presence of wetting and drying. With the inclusion of all upwind surface flux that may impact the mass balance at a river confluence grid, allocations of discharge between the confluence grid and downstream tributaries are achieved under the control of the water depth gradient while ignoring the momentum loss. Momentum loss is also neglected at the river–floodplain interface, and this is a reasonable critique of the scheme, but it is implemented for simplicity. All the results, especially the real-world tests, indicate that the resulting algorithm is numerically stable, relatively simple, and extremely efficient. Together with the separately configured river bathymetry, the new SGC model provides a convenient solution for fine-scale river hydraulics modelling based on a relatively coarse grid, while modelling stability and accuracy are further improved.

Additionally, the examples given demonstrate that the present formulation can generate accurate results, even with a coarse and structured finite-difference mesh, and costly and unnecessary grid refinements are avoided with the subscale representation of river channel bathymetry. Without compromising the computational efficiency, the new solution stencil improved the model performance in terms of water depth distribution and floodplain inundation extent, especially in the case of low-friction scenarios in which abundant smooth urban areas exist. The improved SGC model highlights the vital importance of representing river flow conveyance capacity modelling as well as the mass and momentum exchange over river–floodplain boundaries. Without the river channel bathymetry separately included, the full-dynamic 2D SWE solver based on fine-resolution DEM data consumes high computational resources while demanding a long time for calculation, and the water depth distribution and inundation extent may not be well-presented with the crude treatment of the bathymetry in dg2. Furthermore, the SGC model shows its direct advantage over the full-dynamic 2D model in real-world flood modelling. The resource-consuming 2D SWE solvers demand a relatively small computational time step, which makes them unattractive for flood modelling covering an area up to several hundred thousand square kilometres, while the SGC model with a loose CFL condition can acquire the inundation extent efficiently. Quite different from the fv1 and dg2 solvers, the improved SGC model alleviates the heavy computational burden by including the subgrid-scale river channel. The average computational expense of the dg2 solver is approximately 10 times that of the SGC solver in the real-world test, and fv1 takes 4 times more computational time. The river discretization is decoupled from the overlying floodplain grid, and subgrid bathymetry is explicitly included in the solution scheme, permitting a significant gain in efficiency and accurate simulation of the wetting and drying dynamics. The river hydraulics can be acquired simultaneously with the flood propagation on the floodplain

without resorting to costly and unnecessary grid refinements. The results obtained with coarser grid cell sizes and subgrid sampling are comparable to those obtained with considerably higher grid cell resolution but at a fraction of the computing effort and data storage.

The adaptive weighting factor in the upwind scheme balances the contribution from the local flux and upwind discharge, with a large value importing less upwind diffusion. The feasible range of the weighting factor is determined empirically, as the upwind solution scheme with a fixed weighting factor is sufficiently stable with a minimum of 0.7. Results from Tests 1–3 indicate that a smaller weighting factor can only be acquired at the very beginning of the simulation, and the factor ranges from 0.70 to 0.83 when a steady state is achieved in Test 3. Therefore, confinement is applied to the adaptive weighting factor, which limits its minimum value to 0.70, or a negative volume may be achieved at a river confluence area where three upwind flow discharges are combined to estimate the momentum flux across the cell boundaries. Repeat utilization of the upwind flow discharge for the four cell boundaries may result in an overestimation of the output discharge and affect the model mass balance. Relying heavily on upwind discharge while ignoring local flow slope may accelerate the overall wave propagation speed without any theory evidence. Though an assessment of every cell can be executed to redistribute the discharge once a negative volume is generated, substantial extra computational resources are required. By limiting the minimum value of the adaptive weighting factor, local surface flux is given first priority while updating the momentum exchange for the next time step, and a limited artificial diffusion impact can propagate upwind flow information while avoiding mass errors. A thorough analytical analysis of the optimized range of the adaptive weighting factor may be conducted in future work.

In summary, the new SGC model exhibits its advantage over full 2D SWEs solvers in modelling the river hydraulics and floodplain inundation simulation wherein small-scale river hydraulics have a strong control on the flood generation. With the OpenMP acceleration technology on multi-CPU cores, the SGC model based on the efficient inertial formulation of shallow water equations provides a good approximation of real-world inundation processes and shows great potential in large-scale modelling. With the adaptive upwind diffusion incorporated, potential instability in the case of low-friction scenarios is tackled, and flow conveyance capacity can be modelled with the inclusion of approximate subscale bathymetry, providing a compelling alternative for river–floodplain modelling.

Code and data availability. Code of the improved subgrid channel model is available on Zenodo (<https://doi.org/10.5281/zenodo.7064320>; Rong, 2022), as are the test configuration files that can be used for running the original SGC, improved SGC, and fv1 and dg2 solvers. Water surface

elevation and boundary conditions for the Carlisle test are available in Neal et al. (2009).

Author contributions. YR coded the numerical solvers under the supervision of PB and JN, conducted simulations, and drafted the initial paper. PB and JN gave many suggestions on improving the draft. All authors contributed to conceptualization as well as paper review and editing.

Competing interests. At least one of the (co-)authors is a member of the editorial board of *Geoscientific Model Development*. The peer-review process was guided by an independent editor, and the authors also have no other competing interests to declare.

Disclaimer. Publisher's note: Copernicus Publications remains neutral with regard to jurisdictional claims in published maps and institutional affiliations.

Acknowledgements. Youtong Rong was supported by the China Scholarship Council (CSC)–University of Bristol Joint PhD Scholarship Programme (grant no. 202006250032). Paul Bates is supported by a Royal Society Wolfson Research Merit award and the UKRI Natural Environment Research Council (grant no. NE/V017756/1). Jeffrey Neal is supported by the UKRI Natural Environment Research Council (grant no. NE/S015795/1).

Financial support. This research has been supported by UK Research and Innovation (grant nos. NE/V017756/1 and NE/S015795/1) and the Royal Society (Royal Society Wolfson Research Merit award (grant no. WM170026)).

Review statement. This paper was edited by Simone Marras and reviewed by Ting Zhang and one anonymous referee.

References

Al Baky, M. A., Islam, M., and Paul, S.: Flood hazard, vulnerability and risk assessment for different land use classes using a flow model, *Earth Syst. Environ.*, 4, 225–244, 2020.

Alsdorf, D., Bates, P., Melack, J., Wilson, M., and Dunne, T.: Spatial and temporal complexity of the Amazon flood measured from space, *Geophys. Res. Lett.*, 34, L08402, <https://doi.org/10.1029/2007GL029447>, 2007.

Ayog, J. L., Kesserwani, G., Shaw, J., Sharifian, M. K., and Bau, D.: Second-order discontinuous Galerkin flood model: comparison with industry-standard finite volume models, *J. Hydrol.*, 594, 125924, <https://doi.org/10.1016/j.jhydrol.2020.125924>, 2021.

Bates, P. D., Horritt, M. S., and Fewtrell, T. J.: A simple inertial formulation of the shallow water equations for efficient two-dimensional flood inundation modelling, *J. Hydrol.*, 387, 33–45, <https://doi.org/10.1016/j.jhydrol.2010.03.027>, 2010.

Cook, A. and Merwade, V.: Effect of topographic data, geometric configuration and modeling approach on flood inundation mapping, *J. Hydrol.*, 377, 131–142, <https://doi.org/10.1016/j.jhydrol.2009.08.015>, 2009.

Cozzolino, L., Cimorelli, L., Della Morte, R., Pugliano, G., Piscopo, V., and Pianese, D.: Flood propagation modeling with the Local Inertia Approximation: Theoretical and numerical analysis of its physical limitations, *Adv. Water Resour.*, 133, 103422, <https://doi.org/10.1016/j.advwatres.2019.103422>, 2019.

de Almeida, G. A. and Bates, P.: Applicability of the local inertial approximation of the shallow water equations to flood modeling, *Water Resour. Res.*, 49, 4833–4844, 2013.

de Almeida, G. A., Bates, P., Freer, J. E., and Souvignet, M.: Improving the stability of a simple formulation of the shallow water equations for 2-D flood modeling, *Water Resour. Res.*, 48, W05528, <https://doi.org/10.1029/2011WR011570>, 2012.

Edmonds, D. A., Caldwell, R. L., Brondizio, E. S., and Siani, S. M.: Coastal flooding will disproportionately impact people on river deltas, *Nat. Commun.*, 11, 1–8, 2020.

Fewtrell, T. J., Neal, J. C., Bates, P. D., and Harrison, P. J.: Geometric and structural river channel complexity and the prediction of urban inundation, *Hydrol. Process.*, 25, 3173–3186, <https://doi.org/10.1002/hyp.8035>, 2011.

Grimaldi, S., Li, Y., Walker, J. P., and Pauwels, V. R. N.: Effective Representation of River Geometry in Hydraulic Flood Forecast Models, *Water Resour. Res.*, 54, 1031–1057, <https://doi.org/10.1002/2017wr021765>, 2018.

Horritt, M. S., Bates, P. D., Fewtrell, T. J., Mason, D. C., and Wilson, M. D.: Modelling the hydraulics of the Carlisle 2005 flood event, *Proceedings of the Institution of Civil Engineers – Water Management*, 163, 273–281, <https://doi.org/10.1680/wama.2010.163.6.273>, 2010.

Hunter, N., Bates, P., Neelz, S., Pender, G., Villanueva, I., Wright, N., Liang, D., Falconer, R. A., Lin, B., and Waller, S.: Benchmarking 2D hydraulic models for urban flooding, *Proceedings of the Institution of Civil Engineers-Water Management*, 13–30, 2008.

Hunter, N. M., Horritt, M. S., Bates, P. D., Wilson, M. D., and Werner, M. G. F.: An adaptive time step solution for raster-based storage cell modelling of floodplain inundation, *Adv. Water Resour.*, 28, 975–991, <https://doi.org/10.1016/j.advwatres.2005.03.007>, 2005.

Jongman, B., Ward, P. J., and Aerts, J. C.: Global exposure to river and coastal flooding: Long term trends and changes, *Global Environmental Change*, 22, 823–835, 2012.

Kesserwani, G., Ayog, J. L., and Bau, D.: Discontinuous Galerkin formulation for 2D hydrodynamic modelling: Trade-offs between theoretical complexity and practical convenience, *Comput. Method. Appl. M.*, 342, 710–741, <https://doi.org/10.1016/j.cma.2018.08.003>, 2018.

Leopold, L. B. and Maddock, T.: The hydraulic geometry of stream channels and some physiographic implications, US Government Printing Office, 1953.

McMichael, C., Dasgupta, S., Ayeb-Karlsson, S., and Kelman, I.: A review of estimating population exposure to sea-level rise and the relevance for migration, *Environ. Res. Lett.*, 15, 123005, <https://doi.org/10.1088/1748-9326/abb398>, 2020.

Merwade, V., Cook, A., and Coonrod, J.: GIS techniques for creating river terrain models for hydrodynamic modeling and flood

- inundation mapping, *Environ. Model. Softw.*, 23, 1300–1311, <https://doi.org/10.1016/j.envsoft.2008.03.005>, 2008.
- Neal, J., Schumann, G., and Bates, P.: A subgrid channel model for simulating river hydraulics and floodplain inundation over large and data sparse areas, *Water Resour. Res.*, 48, W11506, <https://doi.org/10.1029/2012WR012514>, 2012.
- Neal, J., Hawker, L., Savage, J., Durand, M., Bates, P., and Sampson, C.: Estimating river channel bathymetry in large scale flood inundation models, *Water Resour. Res.*, 57, e2020WR028301, <https://doi.org/10.1029/2020WR028301>, 2021.
- Neal, J. C., Bates, P. D., Fewtrell, T. J., Hunter, N. M., Wilson, M. D., and Horritt, M. S.: Distributed whole city water level measurements from the Carlisle 2005 urban flood event and comparison with hydraulic model simulations, *J. Hydrol.*, 368, 42–55, 2009.
- Neal, J. C., Odoni, N. A., Trigg, M. A., Freer, J. E., Garcia-Pintado, J., Mason, D. C., Wood, M., and Bates, P. D.: Efficient incorporation of channel cross-section geometry uncertainty into regional and global scale flood inundation models, *J. Hydrol.*, 529, 169–183, <https://doi.org/10.1016/j.jhydrol.2015.07.026>, 2015.
- O’Loughlin, F. E., Neal, J., Schumann, G., Beighley, E., and Bates, P. D.: A LISFLOOD-FP hydraulic model of the middle reach of the Congo, *J. Hydrol.*, 580, 124203, <https://doi.org/10.1016/j.jhydrol.2019.124203>, 2020.
- Paiva, R. C., Collischonn, W., and Tucci, C. E.: Large scale hydrologic and hydrodynamic modeling using limited data and a GIS based approach, *J. Hydrol.*, 406, 170–181, 2011.
- Rajib, A., Liu, Z., Merwade, V., Tavakoly, A. A., and Follum, M. L.: Towards a large-scale locally relevant flood inundation modeling framework using SWAT and LISFLOOD-FP, *J. Hydrol.*, 581, 124406, <https://doi.org/10.1016/j.jhydrol.2019.124406>, 2020.
- Rong, Y.: An improved sub-grid channel model, Zenodo [code], <https://doi.org/10.5281/zenodo.7064320>, 2022.
- Rudari, R., Campo, L., Rebora, N., Boni, G., and Herold, C.: Improvement of the global food model for the GAR 2015, United Nations, Geneva, 2015.
- Schumann, G. J. P., Neal, J. C., Voisin, N., Andreadis, K. M., Pappenberger, F., Phanthuwongpakdee, N., Hall, A. C., and Bates, P. D.: A first large-scale flood inundation forecasting model, *Water Resour. Res.*, 49, 6248–6257, <https://doi.org/10.1002/wrcr.20521>, 2013.
- Sehili, A., Lang, G., and Lippert, C.: High-resolution subgrid models: background, grid generation, and implementation, *Ocean Dynam.*, 64, 519–535, 2014.
- Shaw, J., Kesserwani, G., Neal, J., Bates, P., and Sharifian, M. K.: LISFLOOD-FP 8.0: the new discontinuous Galerkin shallow-water solver for multi-core CPUs and GPUs, *Geosci. Model Dev.*, 14, 3577–3602, <https://doi.org/10.5194/gmd-14-3577-2021>, 2021.
- Shustikova, I., Domeneghetti, A., Neal, J. C., Bates, P., and Castellarin, A.: Comparing 2D capabilities of HEC-RAS and LISFLOOD-FP on complex topography, *Hydrol. Sci. J.*, 64, 1769–1782, 2019.
- Sridharan, B., Gurivindapalli, D., Kuiry, S. N., Mali, V. K., Nithila Devi, N., Bates, P. D., and Sen, D.: Explicit Expression of Weighting Factor for Improved Estimation of Numerical Flux in Local Inertial Models, *Water Resour. Res.*, 56, e2020WR027357, <https://doi.org/10.1029/2020WR027357>, 2020.
- Sridharan, B., Bates, P. D., Sen, D., and Kuiry, S. N.: Local-inertial shallow water model on unstructured triangular grids, *Adv. Water Resour.*, 152, 103930, <https://doi.org/10.1016/j.advwatres.2021.103930>, 2021.
- Trigg, M. A., Wilson, M. D., Bates, P. D., Horritt, M. S., Alsdorf, D. E., Forsberg, B. R., and Vega, M. C.: Amazon flood wave hydraulics, *J. Hydrol.*, 374, 92–105, 2009.
- Trigg, M. A., Bates, P. D., Wilson, M. D., Schumann, G., and Baugh, C.: Floodplain channel morphology and networks of the middle Amazon River, *Water Resour. Res.*, 48, W10504, <https://doi.org/10.1029/2012wr011888>, 2012.
- Yamazaki, D., Kanae, S., Kim, H., and Oki, T.: A physically based description of floodplain inundation dynamics in a global river routing model, *Water Resour. Res.*, 47, W04501, <https://doi.org/10.1029/2010WR009726>, 2011.
- Yamazaki, D., O’Loughlin, F., Trigg, M. A., Miller, Z. F., Pavelsky, T. M., and Bates, P. D.: Development of the Global Width Database for Large Rivers, *Water Resour. Res.*, 50, 3467–3480, <https://doi.org/10.1002/2013wr014664>, 2014.